VIRTUAL AND PHYSICAL SIMULATION OF MULTI-AXIAL FORGING PROCESSES

JÓZSEF B. RENKÓ¹ – PÉTER BERECZKI² – GYÖRGY KRÁLLICS³

Abstract: On a Gleeble 3800 thermo-physical simulator, multi-axial forging of high-purity copper workpieces were performed. The strain rate during the simulation process was 0.1 s⁻¹. The force response and the geometric changes of the workpiece as a function of time were continuously recorded. For a deeper understanding of the multi-axial forging process, a finite element model was created in Qform3D, analysing the changes in the deformation history. In the virtual model, tool movements were controlled using the recorded data of physical simulations. The force-displacement curves of the physical and finite element simulation were compared. The measured and simulated temperature and force values were used to verify the finite element model.

Keywords: multi-axial forging, simulation, finite element, Gleeble, modelling

INTRODUCTION

The technology of severe plastic deformation (SPD) has undergone significant development over the last 25 years. Various methods have been invented, such as equal channel angular pressing (ECAP) [1–4], high-pressure torsion [4, 5], cyclic extrusion-compression processes [6, 7], cyclic closed die forging [8], or multi-axial forging [9–12]. Due to its easy setup, multi-axial forging is one of the easiest to implement severe plastic deformation technology. Another advantage of multi-axial forging is the possibility to forge workpieces of even up to the size of 50–100 mm.

For the physical realisation of multi-axial forging, a Gleeble 3800 thermo-physical simulator equipped with a MaxStrain unit was used. In a Gleeble system, multiple parameters can be controlled with high precision during the entire forming process, like tool movements, forming speeds, forming forces and temperatures. An additional camera was built into the system to track the deformed geometry.

For a deeper understanding of the process, the performed physical simulations were also created in a finite element simulation. The simulations were created with

Budapest University of Technology and Economics, Department of Materials Science and Engineering, H-1111 Budapest, Hungary renko.jozsef@edu.bme.hu

Institute of Engineering Sciences, University of Dunaújváros H-2401 Dunaújváros, Hungary bereczkip@uniduna.hu

Institute of Physical Metallurgy, Metal Forming and Nanotechnology, University of Miskolc H-3515 Miskolc-Egyetemváros, Hungary femkgy@uni-miskolc.hu

QForm3D. The proper use of the finite element simulation could allow studying the whole forging process at any moment. With a well-prepared virtual model, real conditions can be simulated with high accuracy [13–15]. Using finite element simulations before production or physical testing, defects and failed locations could be eliminated almost without exception, even during the design phase [16, 17].

We aimed to reproduce the non-monotonous deformation history of multi-axial forging in a finite element simulation and then to evaluate its reliability. Different characteristic curves of the physical and finite element simulation were compared using the data recorded during both processes.

1. MATERIALS AND METHODS

1.1. Material

The chosen material was an industrial-grade, pure copper. The composition of the material was within the prescribed limits. The chemical composition of the substance is shown in *Table 1*.

 Table 1

 Chemical composition of the studied CuE material

Element	Cu	Fe	Pb	S	Zn	Ni	Sn
Conc.	99.978	0.005	0.004	0.004	0.004	0.002	0.002
(atomic%)	99.910	0.003	0.004	0.004	0.004	0.002	0.002

The chosen material must be suitable for cold forming, in which deformation was not held back by precipitations. CuE is a high-purity industrial copper with a minimum ratio of alloys and contaminants, making it ideal for the selected tests.

1.2. Programming of Gleeble thermo-physical simulator

Multi-axial forging was performed on the MaxStrain unit of the Gleeble 3800 thermo-physical simulator. The workpiece was to be forged in ten steps. The equivalent plastic strain achieved in each forming step was 0.4. Thus, the cumulative strain at the end of the process was 4. During the simulation, the middle, $12 \times 12 \times 12$ mm size part of the square cross-sectional volume was forged with flat-faced, 10 mm wide tools. The workpiece was secured with clamps, connected to a manipulator, allowing the workpiece to be rotated along its longitudinal axis. The multidirectional cyclic deformation is thus carried out by the same tool, with the manipulator rotating 90° on the workpiece between each forming step (*Figure 1*).

The simulator continuously records tool movements, force and temperature according to the previously set 100 Hz measurement frequency. By programming the simulator, the dimensions of the workpiece between the forging steps can also be recorded. To accurately determine the dimensions of the workpiece, preforming is necessary at a rate of 0.1 s⁻¹ before each forging steps. The equivalent plastic strain of the preforming was set to 0.1. This is necessary because the free surfaces of the workpiece start barrelling during forging. At the beginning of each step, the contact

surface between the workpiece and the tool would be irregular, causing also irregular force. The phenomenon could be corrected by suppressing the barrelled surfaces of the workpiece with the small plastic deformation described previously between the main forming steps.

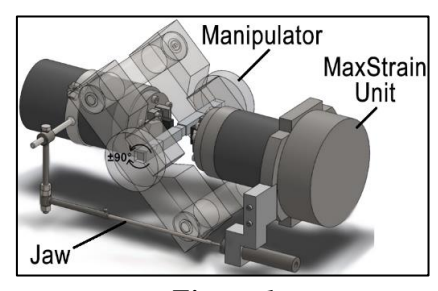


Figure 1
Conceptual setup of MaxStrain unit and the workpiece rotating manipulator

The system has been augmented with an integrated camera that allows the geometry of the workpiece to be captured in snapshots before and after each forming steps. The pictures recorded during the shaping steps are shown in *Figure 2*.

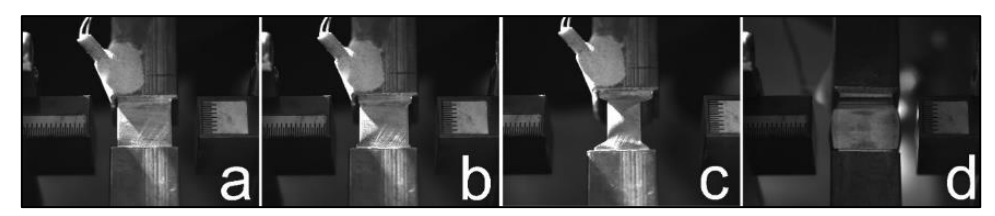


Figure 2

Pictures recorded by the camera between steps: before pre-forming (a), after pre-forming (b), after main forming (c), rotated with 90° after main forming (d)

To record the changes of the temperature, a thermocouple was fixed into the work-piece as shown in the top left corner in Figure~2. The binder used to secure the thermocouple had to be heated up to $100~^{\circ}$ C. Due to the excellent thermal conductivity of copper, the entire workpiece was heated, so it must be cooled before the experiments. The forging experiments were thus started at $30~^{\circ}$ C.

2. FINITE ELEMENT SIMULATION

Finite element simulations of the process were performed with QForm3D 9.0.8. software. The CAD model of the workpiece, tools and fixing clamps were previously created to support the simulation. To reduce the computational time, a half-model was used. Further simplification of the workpiece, possibly a quarter or eighth model was not applicable due to the design of the mounting clamps (*Figure 3*).

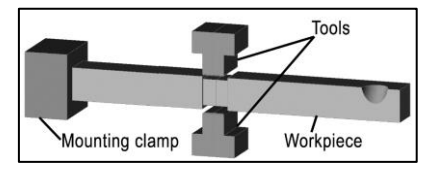


Figure 3
Workpiece clamping and tool placement

2.1. Determination of tool movements

In the virtual simulation, the rotation of the workpiece was simplified by defining two additional tools. While one of the tool pairs performed the active forming step, the other tool pair waited in the rear end position. After forging, the active tools returned to their rear end position. The active and passive tools were then interchanged, and the next forming step has begun.

Using the time-displacement value pairs recorded during multi-axial forging, tool-paths in different directions were created. Jaw recorded the relative displacement of the two tools from each other since the measurement started (*Figure 4*). Positive values indicate the convergence of the tools, while negative values indicate the distancing. In the Gleeble simulator, at the rear end position of the tools, the Jaw was set to –21 mm. This is due to the need to maintain sufficient distance between the tools and the workpiece during rotations, thus protecting the machine from collisions. Examining the displacement curve, the ten shaping steps have a total of thirty characteristic peaks. For each forming step, the first of the three vertices is the preforming, the second is a thickness measured perpendicular to the direction of the current forming step, and the third one is the main forming.

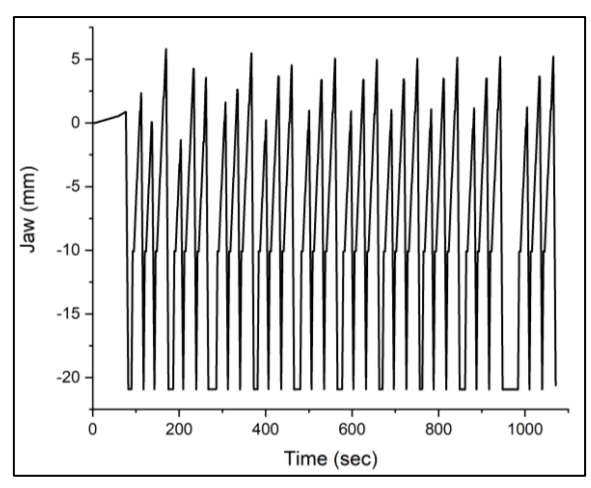
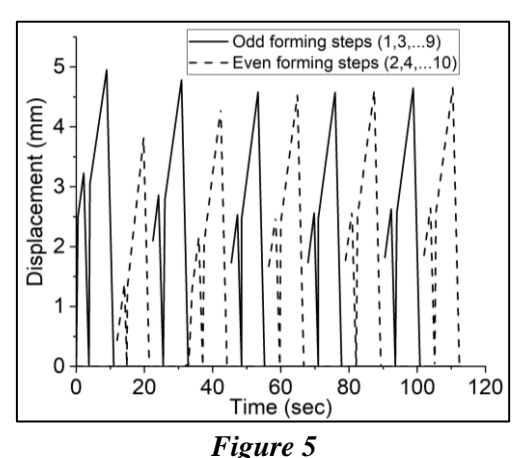


Figure 4
Relative tool distance recorded by Jaw

The tool-paths have been modified so that in their rear end position, the tools do not reach the deforming workpiece, nor do they move unnecessarily far. Based on the data recorded by the Gleeble simulator, the optimal rear end position was determined to be at -2.5 mm from the surface of the unformed workpiece. The dead time thus released was also removed from the tool movements. Pre-positioning tool movements, preforming, and measuring movements were also neglected. The curve describing the relative displacement of the tools is shifted along the y-axis so that at point 0 the surface of the tool and the unformed workpiece touch each other. Finally, the resulting curve was divided into two parts and its value was halved depending on the direction from which the forming is taking place. The resulting tool-paths are shown in *Figure 5*. The curves thus obtained were used to describe the tool movements over time.



Tool movements as a function of time

2.2. Additional settings

The meshing of the bodies was created automatically by the QForm3D system using the previously set boundary conditions. The mesh density was set to finer in the environment of the clamp and the deformation area, while coarser in the stem of the workpiece. Using this mesh, the planned measurement accuracy was achieved, while the computation time did not increase significantly (*Figure 6*). The re-meshing during the simulation was continuous and automatic, preserving the boundary conditions, as well as further increasing the mesh density in the plastic deformation zone. The number of initial nodes was thus 6,049, while the number of initial elements was 32,213. The number of elements and nodes has been constantly changing with remeshing. The maximum number of elements was 80,373 and the maximum number of nodes was 14,448.

As previously described, we aimed to study the reliability of the material model used in general. The material model used in the simulations was CuE, available from the software database. In the adjusted elastic-plastic material model, the flow stress was the function of strain, strain rate and temperature. Thus, thermo-physical aspects

were also considered during the simulation. The initial temperature was set to 30 °C according to the actual measurement conditions.

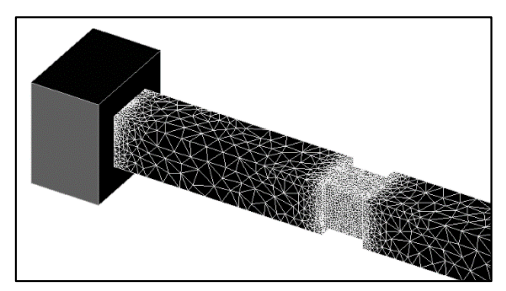


Figure 6
The initial meshing of the workpiece

3. RESULTS AND DISCUSSION

3.1. Force and displacement

Using the force-time-displacement values recorded by the Gleeble simulator, we decomposed the measurement data into ten forming cycles. The force-displacement values experienced during the physical simulation are shown in *Figure 7.a.* The force required for the odd forming steps was significantly higher at the beginning than for the even shaping steps. The dislocation structure formed in the first forming step was less resistant to stress from other directions [18, 19]. The dislocation structure formed in the previous forming step was rearranged depending on the new direction of load. As the forging steps progress, the grain structure of the copper refines, and the curves get closer and closer to each other. The phenomenon is similar to that observed for aluminium alloys studied by Bereczki et al. [18–20].

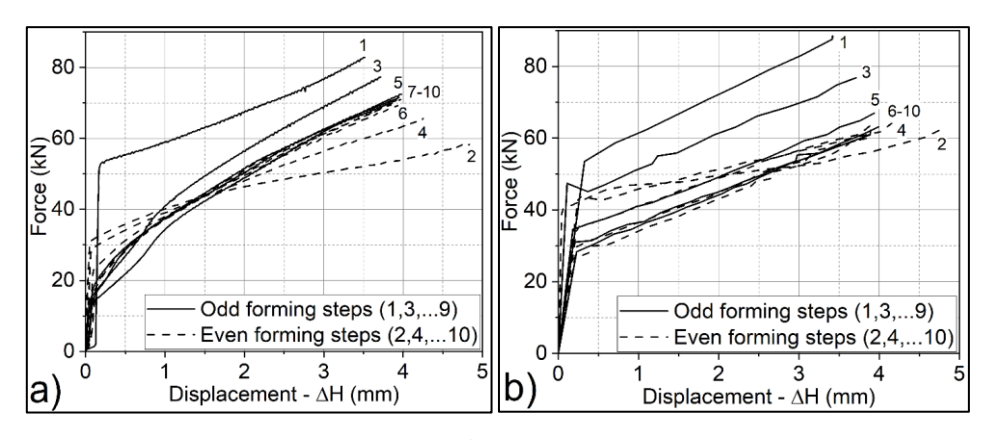


Figure 7

The force as a function of the displacement during physical (a) and finite element (b) simulation

Evaluating the results of the finite element simulation, force-displacement values were recorded (*Figure 7.b*). The curves showed similar characteristic to the force-displacement curves of the physical simulation. However, fitting the curves of the two simulations to each other, the difference emerges (*Figure 8*).

During the first and second forging steps, the finite element simulation assigned higher force values for the same displacements than the physical simulation. During the third and fourth forging steps, the two simulations converged to the same force values, while from the fifth step, the previously observed trend was reversed. The physical simulation required a force approximately 5 kN higher than the finite element simulation.

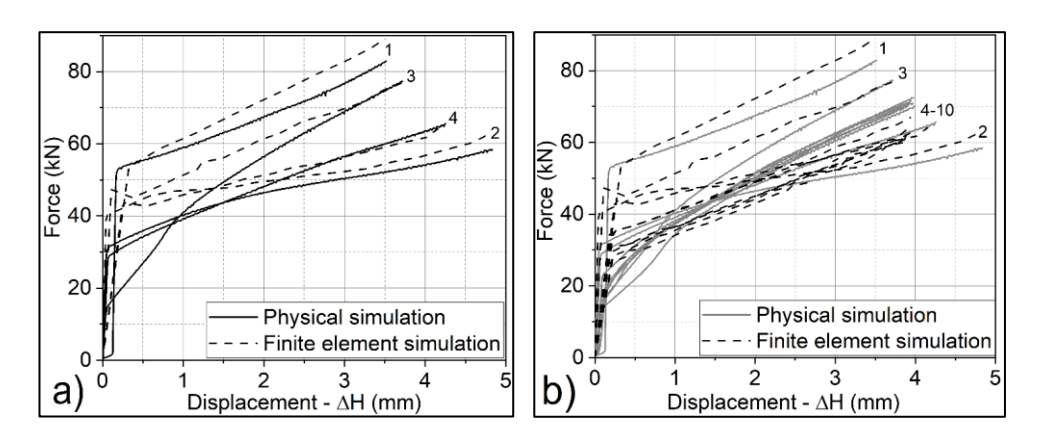


Figure 8
Force-displacement curves recorded during the first four forging steps (a) and during the whole (b) physical and finite element simulation

The reversal of the force curves' trend could be caused by the processes changing the microstructure. Under real conditions, by increasing the cumulative plastic strain, significant grain refining takes place in the forged volume. As a result of the grain refinement, the resistance of the material against deformation increased. Consequently, the force requirement also increased. However, the finite element model did not calculate with such changes in the microstructure, therefore, it couldn't apply its effects.

3.2. Temperature

The temperature change was recorded in both simulations. During the physical simulation, the temperature was measured with a thermocouple. It was embedded into a hole drilled adjacent to the deformation zone. During the finite element simulation, the temperature change was retrieved at the same position as the end of the thermocouple (*Figure 9*).

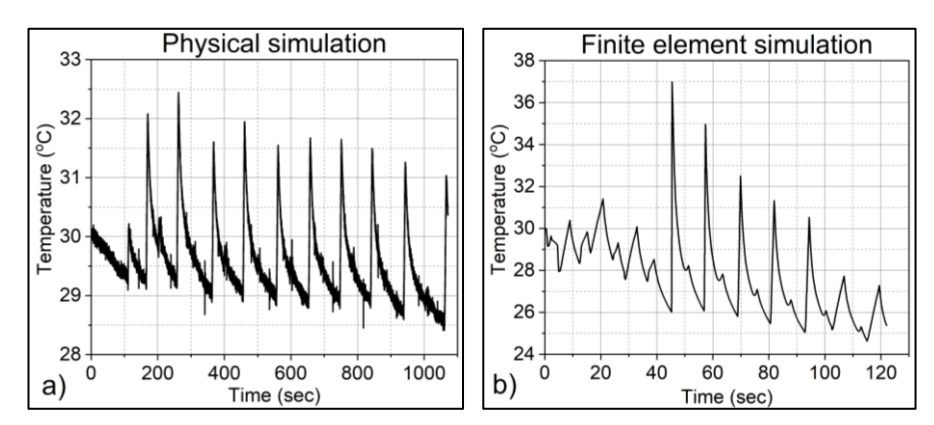


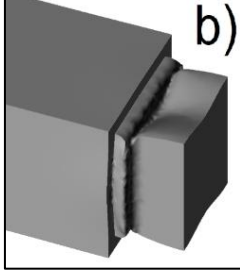
Figure 9
Temperature change recorded during physical (a) and finite element
(b) simulations

Although the temperature curves are very similar, the heat released during forging is much larger in the virtual simulation. This is due to the difference in running time. The finite element simulation ran in 122 seconds, while the physical simulation required nearly 1,100 seconds. With significantly larger tool movements, rotations and measurements, the workpiece have time to transfer heat to its surroundings, so the temperature increase during the physical simulation is less intense.

3.3. Deformed shapes

Copper showed an interesting deformation during multi-axial forging. The usual barrelling in uniaxial compression tests was only observed during the first step. From the second forming step, the thickness of the formed volume continuously decreased inward (*Figure 10*).





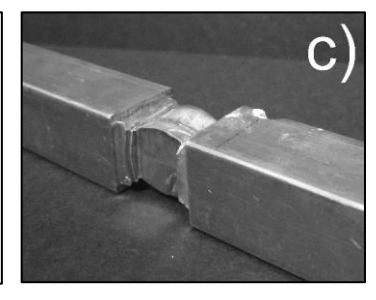


Figure 10

The geometry of the workpiece in the physical simulation (a) and in the finite element simulation (b) after the second forging step.

The geometry of the workpiece after the whole multi-axial forging process (c)

The phenomenon became less and less characteristic as the forming progressed, the material in the middle became more and more resistant to the deformation as the accumulated plastic strain increased. The phenomenon was visible even after the whole forging process ($Figure\ 10.c$). In contrast to the physical simulations, the previously presented mode of deformation in the finite element simulation was maintained throughout. It did not deviate significantly from the shape shown in $Figure\ 10.b$ even after the tenth step.

CONCLUSION

To summarise the results of the study, the implemented finite element simulation was able to reproduce the physical simulation's results with a good approximation. The temperature change, during both processes, moved within a narrow range, so its effect did not cause any significant differences. The force-displacement curves showed a similar nature in both cases. Compared to the first forging step, the second forging step required significantly less force. After the second forging step, the curves run in the region bounded by the first and second curves, getting closer and closer to each other. Assuming the existence of the force-displacement curve of the theoretical, infinite forging cycle, from the third forging step the odd-numbered force-displacement curves approach that from above, and the even-numbered curves approach that from below.

When comparing the force-displacement values, the curves recorded in the virtual simulation showed higher force necessity during the first couple of forging steps. However, with increasing cumulative plastic strain, the trend was reversed and showed lower force values at the same displacement than the physical simulation. The differences between the force curves could be traced back to the applied material model. As the cumulative plastic strain increased, the geometry of the finite element model also differed more and more from that observed in the physical simulator. The used material model was presumably unable to trace the refinement of the grain structure and the increase in strength associated with the dislocation structure arranging in different directions.

Most of the parameters set in the finite element simulation could be suitable for studying the process of multi-axial forging. To do this, however, critical elements, such as the material model need to be redesigned specifically for multi-axial forging. By setting up a material model suitable to describe the changes during multi-axial forging, we could gain a more in-depth insight into the processes using virtual simulations.

ACKNOWLEDGEMENT

This study was supported by the Hungarian Scientific Research Fund, OTKA, Grant No. K-119566. The results presented in this paper are part of a research work, which is also supported by the EFOP-3.6.1-16-2016-00003 project of Hungarian Government, called *The long term collaboration of the R&D processes* at University of Dunaújváros.

REFERENCES

- [1] Segal, V. M., Reznikov, V. I., Drobyshevkij, A. E., Kopylov, V. I. (1981). *Russian Metallurgy*. 1, p. 115.
- [2] Segal, V. M. (1995). Materials processing by simple shear. *Mater. Sci. Eng. A*, 197, pp. 157–164.
- [3] Segal, V. M. (2004). The development of essentials of material processing by severy plastic deformation. *Metally*, 1, pp. 5–14.
- [4] Valiev, R. Z., Islamgaliev, R. K., Alexandrov, I. V. (2000). Bulk nanostructured materials from severe plastic deformation. *Progress in Mater. Sci.*, 45, pp. 103–189.
- [5] Popov, A. A., Pyshmintsev, I. Y., Demakov, S. I., Illarionov, A. G., Lowe, T. C., Valiev, R. Z. (1997). Structural and mechanical properties of nanocrystalline titanium processed by severe plastic deformation processing. *Scr. Mater.*, 37, pp. 1089–1094.
- [6] Korbel, A., Richert, M., Richert, J. (1981). The effects of very high cumulative deformation on structure and mechanical properties of aluminium In: *Proc.* 2nd Riso Int. Symp. on Metallurgy and Material Science, Roskilde, Denmark, September 14–18, pp. 445–450.
- [7] Zrnik, J., Dobatkin, S. V., Mamuzi, I. (2008). Processing of metals by severe plastic deformation (SPD) structure and mechanical properties respond. *Metalurgija*, 47 (3), pp. 211–216.
- [8] Magalhães, D., Pratti, A., Kliauga, A., Rubert, J., Ferrante, M., Sordi, V. (2018). Numerical simulation of cryogenic cyclic closed-die forging of Cu: Hardness distribution, strain maps and microstructural stability. *Journal of Materials Research and Technology*, 8 (1), pp. 333–343.
- [9] Szabó, P. J., Bereczki, P., Verő, B. (2011). The Effect of Multiaxial Forging on the Grain Refinement of Low Alloyed Steel. *Periodica Polytechnica Mechanical Engineering*, 55 (1), pp. 63–66.
- [10] Naser, T. S. B., Krállics, G. (2012). The effect of multiple forging and cold rolling on bending and tensile behavior of Al 7075 alloy. *Mater. Sci. Forum*, 729, pp. 464–469.
- [11] Tikhonova, M., Dudko, V., Belyakov, A., Kaibyshev, R. (2010). The Formation of Submicrometer Scale Grains in a Super304H Steel during Multiple Compressions at 700 °C. *Materials Science Forum*, 667–669, pp. 565–570.
- [12] Ringeval, S., Driver, J. H. (2006). A Comparison of Flow Stress and Microstructure Development of Al Alloys in Plane Strain Compression and Multiple Forging. *Materials Science Forum*, 519–521, pp. 979–984.

- [13] Li, J., Wu, F. (2017). Finite Element Analysis on the Precision Forging of the Semimonocoque. *International Conference on Smart Grid and Electrical Automation (ICSGEA)*, Changsha, pp. 355–357.
- [14] Roque, C. M. O. L., Button, S. T. (2000). Application of the finite element method in cold forging processes. *Journal of the Brazilian Society of Mechanical Sciences*, 22 (2), pp. 189–202.
- [15] Renkó, J. B., Kemény, D., Nyirő, J., Kovács, D. (2019). Comparison of cooling simulations of injection moulding tools created with cutting machining and additive manufacturing. *Materials Today: Proceedings*, 12, pp. 462–469.
- [16] Wangchaichune, S., Suranuntchai, S. (2018). Finite Element Simulation of Hot Forging Process for KVBM Gear. *Applied Mechanics and Materials*, 875, pp. 30–35.
- [17] Behrens, B.-A. (2008). Finite element analysis of die wear in hot forging processes. *Cirp Annals-manufacturing Technology*, 57, pp. 305–308.
- [18] Bereczki, P., Szombathelyi, V., Krállics, G. (2014). Determination of flow curve at large cyclic plastic strain by multiaxial forging on MaxStrain System. *International Journal of Mechanical Sciences*, 84, pp. 182–188.
- [19] Bereczki, P., Szombathelyi, V., Krallics, G. (2014). Production of ultrafine-grained aluminum by cyclic severe plastic deformation at ambient temperature. *IOP Conf. Series: Materials Science and Engineering*, 63 (012140).
- [20] Bereczki, P., Krallics, G., Renkó, J. B. (2019). The effect of strain rate under multiple forging on the mechanical and microstructural properties. *Procedia Manufacturing*, 37, pp. 253–260.